Carbohydrate Polymers 100 (2014) 143–149

Contents lists available at ScienceDirect

Carbohydrate Polymers

journal homepage: www.elsevier.com/locate/carbpol

Electrospun nanofibrous cellulose scaffolds with controlled microarchitecture

Katia Rodríguez[a], Johan Sundberg[b], Paul Gatenholm[b,c], Scott Renneckar[a,d,*]

[a] Department of Materials Science, Virginia Tech, Blacksburg, VA 24060, USA
[b] Wallenberg Wood Science Center, Department of Chemical and Biological Engineering, Chalmers University of Technology, Goteborg SE41296, Sweden
[c] School of Biomedical Engineering and Sciences, Virginia Tech, Blacksburg, VA 24060, USA
[d] Department of Sustainable Biomaterials, Virginia Tech, 230 Cheatham Hall, Blacksburg, VA 24060, USA

ARTICLE INFO

Article history:
Received 1 August 2012
Received in revised form
20 November 2012
Accepted 14 December 2012
Available online 25 December 2012

Keywords:
Cellulose
Scaffold
Porosity
Hydroxyapatite
Bone regeneration
Laser

ABSTRACT

Introducing porosity in electrospun scaffolds is critical to improve cell penetration and nutrient diffusion for tissue engineering. Nanofibrous cellulose scaffolds were prepared by electrospinning cellulose acetate (CA) followed by saponification to regenerate cellulose. Using a computer-assisted design approach, scaffolds underwent laser ablation resulting in pores with diameters between 50 and 300 μm without damaging or modifying the surrounding scaffold area. A new mineralization method was employed in conjunction with microablation using commercial phosphate buffered saline (PBS) to soak carboxymethylcellulose surface-modified electrospun scaffolds. The resulting crystals within the scaffold on the interior of the pore had a calcium to phosphate ratio of 1.56, similar to hydroxyapatite. It was observed that porosity of the cellulose scaffolds enhanced osteoblast cell attachment at the edge of the pores, while mineralization enhanced overall cell density.

1. Introduction

Nanofibrous electrospun materials have been successfully used to mimic ultrafine textured extracellular matrix (ECM) for tissue engineering applications (Li, Laurencin, Ctaerson, Tuan, & Ko, 2002). However, cells live in a complex mixture of pores and ridges with architectures that go beyond the simple nonwoven mesh of electrospun fibers (Stevens & George, 2005). Pores positively influence tissue bridging by allowing inward diffusion of growth factors and ECM proteins, and outward diffusion of waste products (Karande, Ong, & Agrawal, 2004). Up to this point, micro- and macroporosity has been difficult to fabricate directly, limited to solid free form (SFF) fabrication techniques (Hollister, 2005). SFF techniques have made remarkable progress enabling scaffold design and fabrication, as 3D bioplotters or layered sintering techniques have reproduced biological structures directly from computed tomography (CT) scan images (Hollister, 2005). These designs inherently have the porosity required for mass transport, enabling required oxygen gradients, enhancing cell seeding and cell clustering, providing cell direction and integration paths, and optimized mechanical properties based on a given porosity restraint. These controlled designs have shown improvement over non-controlled porogen leaching methods where salt, wax, or some other material imbedded in the scaffold is removed after fabrication (Malda et al., 2004). However, there is a trade-off using SFF methods as the micro- to macroscale scaffold structure can be designed as a perfect mimic, there is little control over the nano- to microscale features of the scaffold. This scale is important because this level of architecture is what cells actually "see". Supporting this hypothesis, Chen, Smith and Ma (2006) illustrated that nanofibers created by liquid phase separation of poly (L-lactic acid) deposited by reverse SFF enhanced cell growth and scaffold uniformity.

Electrospinning of biocompatible polymers is advantageous over phase separation techniques because of the control of fiber characteristics such as diameter and orientation of the nanofibrous mat. It is well documented that spinning biocompatible polymers, like collagen (Buttafoco et al., 2006) and polylactic acid (Zong et al., 2005), from solutions under electric fields create fibers with nanoscale dimensions to serve as tissue scaffolds. Polylactic acid is relatively hydrophobic and requires modification to enhance wetting characteristics for cell seeding and cell adhesion (Grafahrend et al., 2011). Nanocellulose biomaterials have history in biomedical applications as material for wound healing (Czaja, Krystynowicz, Bielecki, & Brown, 2006a; Czaja, Young, Kawecki, & Brown, 2006b) and recently have shown promising results in the tissue engineering field (Bodin et al., 2010; Svensson et al., 2005). Cellulose is a hydrophilic material, but insoluble in water because of extensive hydrogen bonding network. When degraded through hydrolysis, cellulose forms glucose, making the degradation products

* Corresponding author at: Department of Sustainable Biomaterials, Virginia Tech, Blacksburg, VA 24060, USA. Tel.: +1 540 231 7100; fax: +1 540 231 8176.
E-mail address: srenneck@vt.edu (S. Renneckar).

0144-8617/$ – see front matter © 2012 Elsevier Ltd. All rights reserved.
http://dx.doi.org/10.1016/j.carbpol.2012.12.037

Table 1
Atomic composition of the mineralized scaffolds by EDX.

Sample description	C	O	Ca	P	Na	Mg	Ca/P
Mineralized EC	17.75	59.32	11.94	10.08	0.75	0.16	1.18
Porous mineralized EC	20.36	58.66	11.32	9.02	0.47	0.26	1.25
Porous mineralized EC cross section	14.71	46.72	23.47	15.05	0.03	0.05	1.56

bioresorbable. To expand processing options cellulose derivatives like cellulose acetate can be transformed into cellulose by regeneration in alkali without impacting fiber structure (Rodriguez, Renneckar, & Gatenholm, 2011).

Novel techniques that enable control of the nanofibrous design along with controlled pore design would enable tissue engineering of the extracellular matrix. Achieving microscopic pores (>100 μm) in a nanostructured scaffold would mimic natural design constraints that impact cell seeding distribution, cell migration throughout the 3D space, cell signaling, and overall mass transport. Only a few studies have demonstrated controlled microscale ablation by direct-write lasers on cell integration. A summary of different works on microporosity by laser ablation is shown in Supplementary Table 1. These methods utilize a computer drawing to design the pore pattern and a laser to ablate the pattern into the scaffold material providing significant spatial control of the design. Lim et al. (2011) and Rebollar et al. (2011) have described the parameters to create pores by a femtosecond laser on polycaprolactone (PCL) and PCL/gelatin membranes, respectively. McCullen et al. (2010) used a pulsed excimer laser on polylactic acid (PLA) electrospun scaffolds. Their results suggested that cells were well spread and attached due to the micropores. These studies suggested that femtosecond laser pulses can minimize polymer thermal degradation in contrast to conventional lasers due to the short time exposure (Lim et al., 2011). Additionally, increase in mineralization due to the presence of micropores has been observed (McCullen et al., 2010). Nevertheless, the capability of conventional CO_2 lasers to produce microporosity without polymer degradation on electrospun membranes has not been previously evaluated.

In addition to porosity, cell adhesion is influenced by the surface chemistry of the scaffold. It was reported that Ca–P mineralized scaffolds can enhance osteoblast cell adhesion to the scaffold (Gilbert et al., 2000; Zimmermann, LeBlanc, Sheets, Fox, & Gatenholm, 2011). Up until now simulate body fluid (SBF) treatment has been extensively used (Chen et al., 2006; Hofmann, Müller, Greil, & Müller, 2006; Ogino, Ohuchi, & Hench, 1980; Ohtsuki, Kushitani, Kokubo, Kotani, & Yamamuro, 1991; Rodriguez et al., 2011; Tas, 2000; Zimmermann et al., 2011) in the Ca–P mineralization process. Improving upon previous work, the use of commercially available phosphate buffered saline (PBS) solution is employed in the current study as an alternative for biomimetic mineralization.

Computer-assisted design (CAD) of porosity in electrospun scaffolds will help enable in vitro tissue engineering with structure and function that mimics biological tissues, such as nanoscale topographical features and microscale porosity (Stevens & George, 2005). In the present study, we show a novel method of achieving controlled microporosity via CO_2 laser ablation of electrospun scaffolds of cellulose. While other laser studies (Table 1) used significantly faster pulsed lasers, we demonstrate that common CO_2 engraving lasers with a microsecond pulse rate can modify cellulose acetate with designed porosity of suggested optimum pore size in the 100–300 μm range (Karageorgiou & Kaplan, 2005). The present study shows a novel pathway to manipulate polysaccharides, such as cellulose, into tissue scaffolds with controlled porosity and surface chemistry. Manipulating polysaccharide fibers into architectures that allow for mass transport, while maintaining the nanoscale features similar to the extracellular matrix will provide a new pathway to utilize these natural materials in tissue engineering applications.

2. Experimental

2.1. Scaffold fabrication

Cellulose scaffolds were produced by electrospinning cellulose acetate (CA, M_n = 30,000 and DS = 2.5) (Sigma–Aldrich). CA solution of 17% (w/w) in 2:1 ratio of acetone/dimethylacetamide (DMAc, 99.9% Sigma–Aldrich) was employed in the electrospinning process. CA solution was fed at 3 mL/h with a syringe pump (Harvard Apparatus) through stainless steel needle with diameter of 0.643 mm (Howard Electronic Instruments Inc.) The needle was connected to a high voltage power supply (Spellman's CZE1000R) and positively charged. A voltage of 25 kV was applied between the needle and the grounded collector, in a horizontal collection set-up. The distance between needle and collector was 10 cm. The electrospun CA fibers were deposited on an aluminum mandrel covered with aluminum foil at 22 °C and 60% RH. The electrospun mats, ca. 150 μm thickness, were handled with gloves (in case of residual solvent) and peeled from the collector.

2.2. Scaffold modification

Porosity was created on the CA fibrous meshes using a direct-write 60 W laser (CO_2 laser of 10 μm wave length, Universal Laser Systems V460) at standard room conditions. The laser has a CO_2 air-cooled cartridge and a high power density focusing optics attachment that allows the laser beam to be focused to spot size of ~32 μm. The porosity was created using the vector mode of the device by controlling the power (W), speed (in/s), and intensity of the laser (pulse per inch, PPI). The porosity patterns were ablated on the electrospun CA samples by using an *x*–*y* axis stage. Pores of approximately 300 μm in diameter, and 300 and 600 μm of separation were ablated on the electrospun CA using 6 W, 6.7 in/s, and 500 PPI. The scaffolds were regenerated to cellulose by saponification reaction with 0.05 N NaOH solution in ethanol at room temperature for 24 h as described in previous study (Rodriguez et al., 2011). In order to enable calcium phosphate crystal growth, the surface of cellulose fibers were modified with carboxyl groups by means of carboxymethyl cellulose (CMC, Mw = 100,000 and DS = 1.2) (Celco, Sweden) adsorption. This process involved the mixture of 0.01 M $CaCl_2$ solution and 125 mg of CMC for 24 h. Subsequently, the scaffolds were treated with 0.1 M $CaCl_2$ solution for 24 h. The modified scaffolds were then placed into deionized water for 1 h and agitated every 15 min. Finally, CMC treated cellulose scaffolds were exposed to phosphate buffered saline solution (PBS, Dulbecco's phosphate-buffered saline with magnesium and calcium, PAA) at 37 °C for 7 days in order to mineralize the cellulose fibers with hydroxyapatite (HA) like crystals. The scaffolds rinsed several times with DI water and sterilized in an autoclave at 121 °C and 230 kPa for 30 min after mineralization.

2.3. Cell study procedure

Mouse osteoprogenitor cells, MC3T3-E1, from American Type Culture Collection (ATCC) (subclone 4, CRL-2593, passage 21) were

expanded in α-modified minimum essential medium (α-MEM, Invitrogen) substituted with 10% (v/v) fetal bovine serum (FBS, PAA) and 1% (v/v) antibiotic/antimyotic (A/A, Invitrogen) in an incubator at 37 °C in 5% CO_2 and 95% relative humidity. After 3 days of expansion the cells had reached 80% confluency. The cells were washed twice with PBS (Dulbecco's phosphate-buffered saline without magnesium and calcium, PAA) and removed from the Petri dishes by treatment with 0.05% (v/v) trypsin–EDTA (Invitrogen). Before cell seeding, the scaffolds were pre-treated for 12 h in α-MEM and incubated at 37 °C in 5% CO_2 and 95% relative humidity to equalize conditions. MC3T3-E1 cells were seeded using a pipette onto the cellulose scaffolds (6 mm of diameter) with a density of 20,000 cells/cm^2 on each scaffold type. The experiment had 2 replicates for each category and the cell study ran for 3 days. Cell seeded samples were fixed with 4% (v/v) methanol free formaldehyde (Polysciences) for 30 min and washed twice with PBS to remove non-adherent cells. Cells were then permeabilized in PBS containing 0.1% Triton-X 100 for 45 min. In order to visualize fixed cells on the scaffolds, the samples were stained with 4′,6-diamidino-2-phenylindole (DAPI) and rhodamine phalloidin to observe nuclei and F-actin of cytoskeleton, respectively.

2.4. Characterization

The morphology of the nanofibrous scaffold was characterized by scanning electron microscopy (SEM, LEO Ultra 55 FEG). Water contact angle (θ) of regenerated electrospun cellulose samples was determined using a First Ten Angstroms contact angle analyzer. Samples were dried in a vacuum oven at 80 °C and 10 mTorr over night before characterization. The contact angle measurements were carried out in regenerated non-woven meshes with size of 2 cm × 6 cm placed onto an object slice. Fourier transform infrared spectroscopy (FTIR, 8700 Nicolet Thermo Electron) in transmission mode, was used in the wavenumber range of 4000–500 cm^{-1} to analyze the chemical structure of the CA scaffolds before and after laser ablation treatment. The composition and structure of the crystals produced by mineralization process were analyzed by SEM (FEI Quanta 600 FEG)-Energy Dispersive X-Ray Spectrometer (EDX, Bruker QUANTAX 400 with high speed silicon drifted detector) and X-ray diffraction (XRD, Bruker D8 Discover). The chemical structure of the crystals produced by the PBS treatment was determined by X-ray diffraction (XRD, Bruker D8 Discover). Porous and non-porous electrospun cellulose (EC) samples were analyzed from 2θ values of 10–60°. Synthetic HA (Sigma–Aldrich) was also characterized by XRD and used as a HA reference. The synthetic HA was indexed using a powder diffraction files. Cell–scaffold interaction was visualized by fluorescence phase contrast microscope (Leica DMI4000 Digital Microscopes Inverted and analyzed in the software Leica LAS AF). Cell density was calculated from fluorescence micrographs using Image J software in order to quantify cell adhesion on the cellulose scaffolds; eleven different images were analyzed per scaffold type.

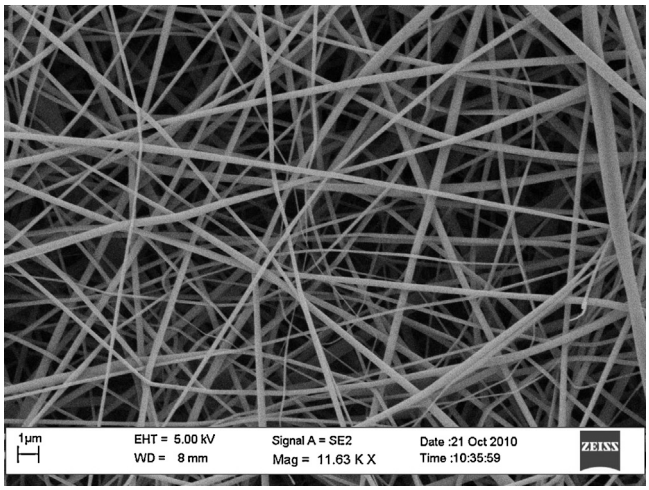

Fig. 1. Electrospun cellulose acetate regenerated into cellulose.

3. Results and discussion

3.1. Morphology and porosity

Chemical modification of cellulose into acetate derivatives changes the solubility of the polymer and the subsequent avenues to process it into films or fibers. Cellulose acetate was electrospun into the submicron scale fibers and then regenerated into cellulose (Fig. 1). After regeneration mean fiber diameter of the electrospun cellulose was 628 nm and the range of 116 nm to 2.4 µm, with the lower value similar to the values encountered for native ECM. The electrospun material forms stable nonwoven scaffolds with relatively high surface area that can be easily wetted by cell culture media. This phenomenon is demonstrated as electrospun fibers from cellulose acetate, regenerated to cellulose, have an extremely low contact angle of less than 20° (Supplementary Fig. 1). Such wetting characteristic of scaffolds is a prerequisite for cell adhesion and to limit non-specific protein binding (Grafahrend et al., 2011).

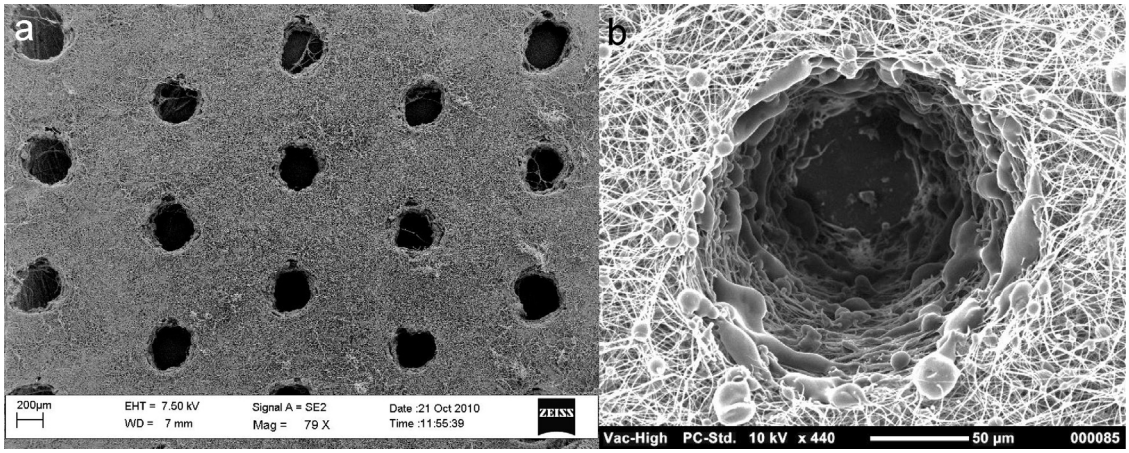

Fig. 2. Micro-ablated electrospun cellulosic scaffolds. (a) Diameters of the pores in pattern are 300 µm. (b) Magnification on edge of 150 µm pore revealing intact fibers.

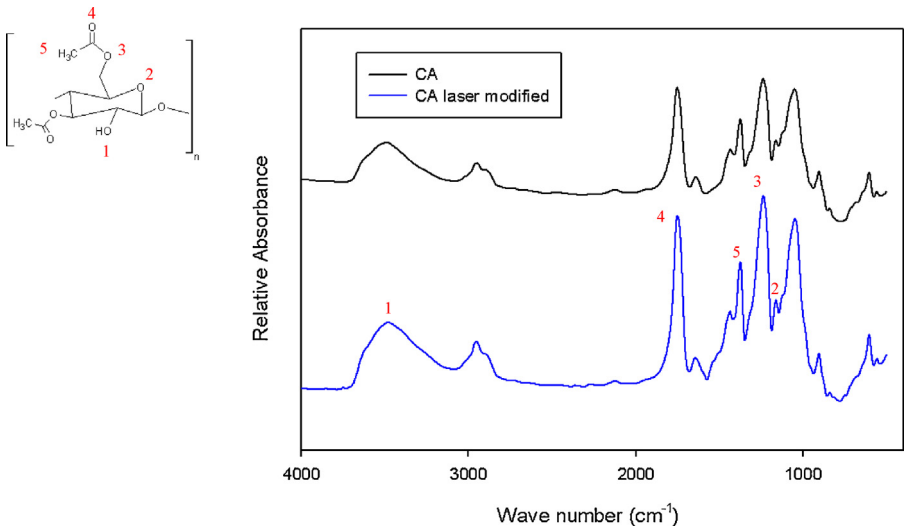

Fig. 3. FTIR spectra of cellulose acetate before and after laser modification.

The overall novelty of using direct-write lasers to engineer the electrospun scaffolds is the limited spread of heat from the high energy density CO_2 laser that can be focused to a spot size that ranges from 50 μm to 70 μm. In general, polymeric fibers are poor heat conductors; in the case of electrospun fibers, the local environment is surrounded by insulating air that limits heat transfer within the scaffold. Electrospun cellulose acetate was irradiated based on a simple pattern of 300 μm pores spaced 600 μm apart (Fig. 2a). As a result of limited heat transfer, fiber degradation only occurred in the irradiated area with minimal changes to the surrounding ultrafine network of fibers (Fig. 2b). From the SEM images there is an indication that the cellulose acetate-based electrospun fibers only underwent localized flow at the pore edge. The laser energy is significantly greater than the thermal degradation temperature transforming the solid material directly into gaseous products leaving no residual solids within the pore and the fiber structure remains intact along the pore edge (Fig. 2b). Additionally, there is no discoloration to the resulting scaffolding indicating that there is no observable char formation (Supplementary Fig. 2), another sign that the material was transformed directly into gaseous products.

To evaluate the possibility of chemical degradation of the electrospun cellulosic membranes due to laser treatment, unmodified and laser treated scaffolds were analyzed by FTIR (Fig. 3). The spectra for the laser treated scaffolds contain chemical information arising from both regions of laser-modified and non-modified cellulose acetate. FTIR spectrum of the CA electrospun material showed the characteristic bands attributed to the vibrations of the acetate group: the carbonyl stretching at 1750 cm^{-1} (νC=O), methyl bending at 1370 cm^{-1} (δC—CH_3), and alkoxyl stretch of the ester at 1235 cm^{-1} (νC—O—C) (Liu & Hsieh, 2002; Ma & Ramakrishna, 2008; Ma, Kotaki, & Ramarkrishna, 2005). The acetal linkages of the cellulose backbone can be observed around 1160 cm^{-1}, the methylene asymmetric stretching at 2853 cm^{-1} (Carrillo, Colom, Suñol, & Saurina, 2004) and the broad hydroxyl group absorption at approximate 3400 cm^{-1} (Liu & Hsieh, 2002). It was observed, by comparison of the spectra, that no significant changes were induced by the laser treatment. Since visual observation, along with FTIR results, did not suggest any detectable chemical modification due to the laser treatment, the non-fibrous material observed at the edge of the pore (Fig. 2b) could be the CA polymer that under went flow during the laser ablation process. Consequently, it was concluded

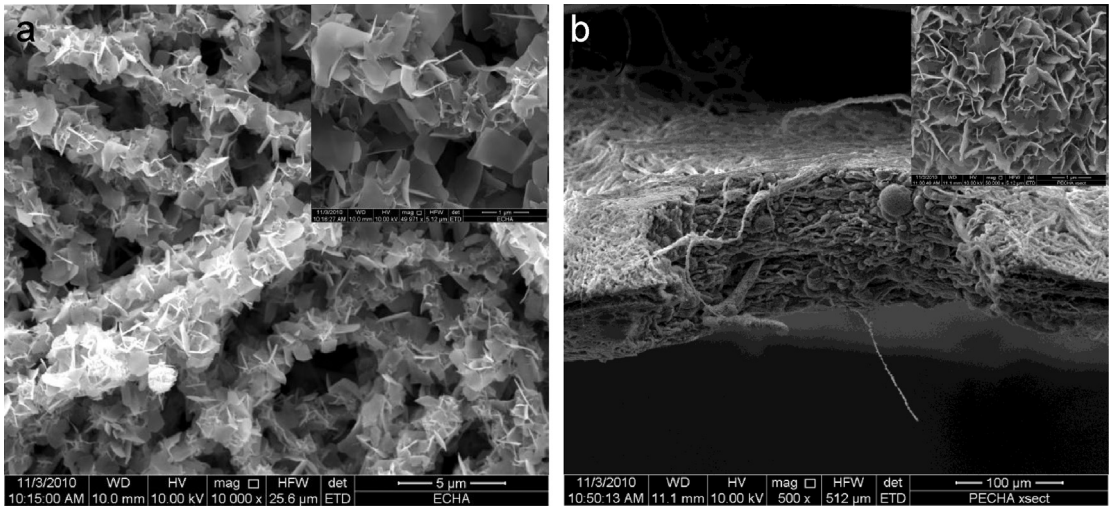

Fig. 4. Surface of electrospun scaffold mineralized in phosphate buffer saline for 1 week. (a) Surface of scaffold, and (b) inner pore of micro-ablated sample. Inset images reveal higher magnification of the flake-like, high surface area, Ca–P minerals.

that it is possible to create microporosity on CA electrospun material by CO_2 laser without bulk thermal degradation of the material. The relevance of this result lies in the decrease of the cost of scaffold fabrication by using a conventional laser and ease of manufacture of microporosity in contrast to femtosecond and pulse excimer lasers.

3.2. Ca–P mineralization

The CA electrospun samples were saponified with 0.05 N NaOH for 24 h to produce cellulose scaffolds. The surface of the cellulose fibers within the scaffold was mineralized after pretreatment in CMC and $CaCl_2$ solution, and subsequent exposure in phosphate buffered saline (PBS) solution for 7 days (Fig. 4a). The crystals have a flake like structure; the large amount of crystals increased the fiber diameter, as can be observed by comparing images in Figs. 2b and 4a. The high magnification inset image in Fig. 4a indicates an increase in surface area, where the 2D flake-shaped crystals are extensions of small area of the fiber. Crystals on the porous electrospun cellulose scaffold were formed not only on the fibers of the scaffold surface but also within the pores (Fig. 4b). The composition of the mineralized scaffold was evaluated by energy dispersive X-ray analysis (EDX). The main components detected by this technique were O, C, Ca, and P with traces of Na and Mg, data shown in Table 1. The atomic composition of these elements was slightly different for the non-porous and porous (laser ablated) materials. The concentrations of C and Mg were 1.4-fold and 1.6-fold higher, respectively, for porous mineralized scaffolds. In contrast to the fibers on the surface of the scaffold, the inner pore surface (within the same sample) has twice and 1.7 times higher concentrations of Ca and P without any Na and Mg. As a result the Ca/P ratio calculated from the EDX data for non-porous and porous mineralized scaffolds were 1.18 and 1.25, respectively. However, lining the inner pore surface the Ca/P ratio was 1.56, which is close to 1.67, the value of hydroxyapatite crystals (Posner & Betts, 1975).

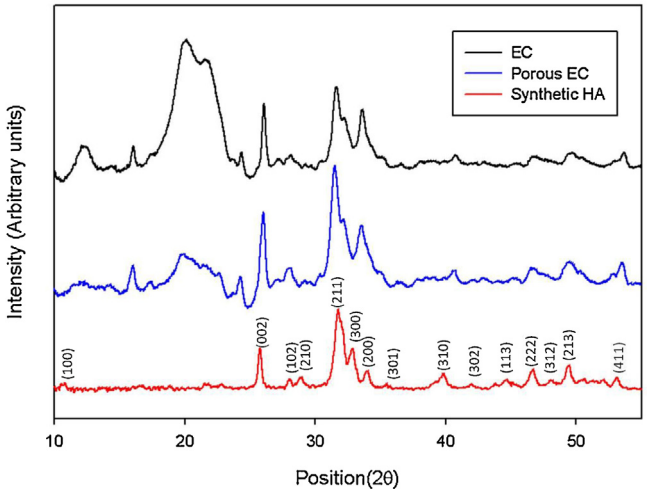

Fig. 5. Powder X-ray diffractograms of mineralized electrospun scaffolds and synthetic HA.

The X-ray powder diffraction pattern of the mineralized scaffold showed peaks similar to synthetic hydroxyapatite (Fig. 5). The peaks located at angles 12°, 20°, and 22° are associated to regenerated cellulose and are characteristic of the crystalline structure of cellulose II. Cellulose II diffraction pattern was expected due to the NaOH treatment during regeneration process of the cellulose acetate nonwoven meshes. The diffraction peaks observed at 2θ equal to 25.8°, 31.8°, 32.9°, 34.0°, 39.7°, 46.6°, 49.4°, and 53.1° correspond to HA as highlighted by the reference spectrum (Fig. 5). The HA XRD peaks were observed for porous and non-porous samples treated with PBS. This result confirms that Ca–P crystals with similar structure to HA were produced on the electrospun fibers due to the PBS treatment. If the X-ray data is compared to previous data

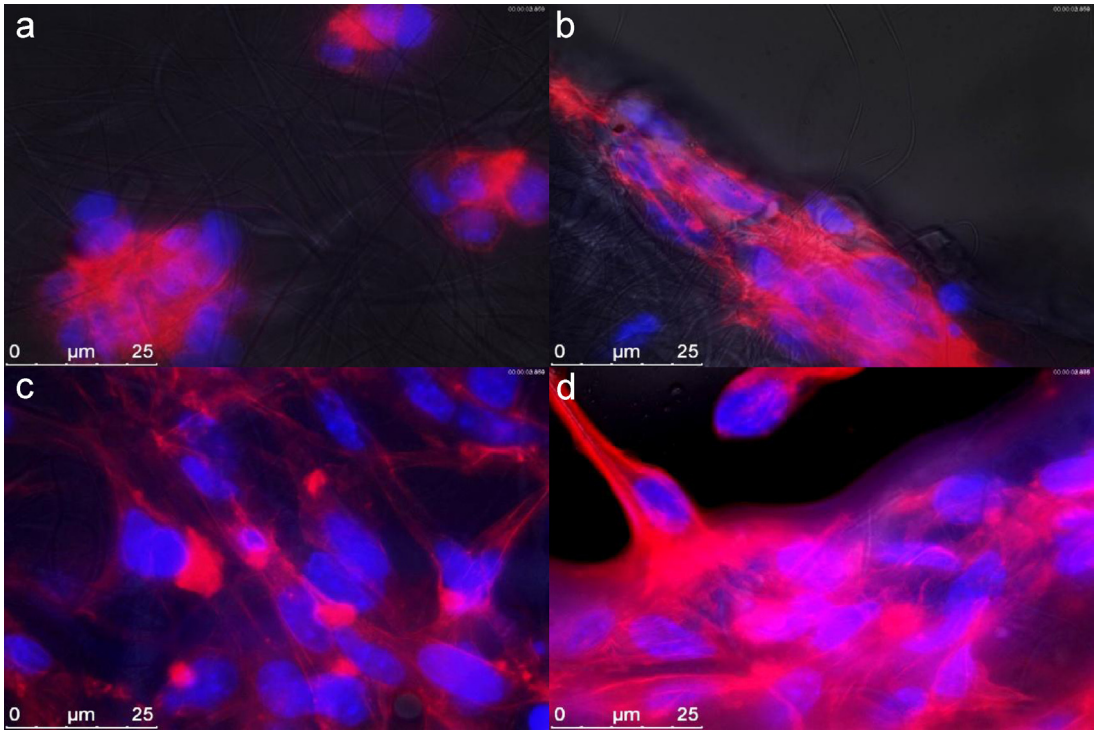

Fig. 6. MC3T3-E1 cells seeded on electrospun scaffolds with their nucleus dyed with DAPI, and F-actin stained with rhodamine phalloidin. (a) Electrospun cellulose scaffold, (b) electrospun cellulose scaffold with cells lining the microablated pore, (c) mineralized electrospun scaffold, and (d) mineralized electrospun scaffold with cells lining microablated pore.

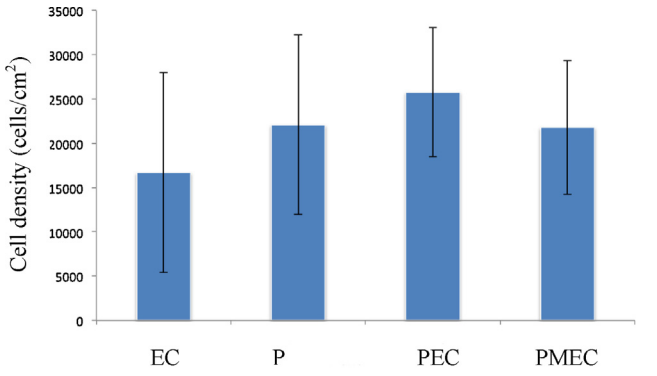

Fig. 7. MC3T3-E1cell density on (a) electrospun cellulose (EC), (b) porous electrospun cellulose (PEC), (c) mineralized electrospun cellulose, and (d) porous mineralized cellulose scaffolds.

with simulated body fluid as the electrolyte solution (Rodriguez et al., 2011), the peaks are sharper in the current study suggesting an increase in crystallite size, as found through the Scherrer equation (Murdock, 1930).

3.3. Cell–scaffold interaction

Osteoprogenitor cells were seeded on the electrospun scaffolds to investigate the scaffolds for potential cytotoxicity and early cell adhesion. The seeded cells were fixed with formaldehyde after 3 days of culture and were stained to highlight the cell nuclei and F-actin of their cytoskeleton. Most of the cells cultured on unmodified electrospun material displayed cluster like morphologies (Fig. 6a). Microscopy results indicated limited adhesion, as there were many regions of the scaffolds that did not host any cells. Additionally, F-actin was not significant indicating minimal stretching of the cells across the scaffold surface. Cells cultured on the porous scaffold showed cell clustering at the pore edges and within the pores. More F-actin appeared in the images for the cells near the pores with some stretching evident as the nuclei were elongated. A large difference in cell morphology was observed for both the mineralized samples relative to the samples that were not surface modified. Cells were stretched over the surface, indicative of good cell adhesion (Fig. 6b–d). This result suggested that cells cultured on mineralized scaffolds bind better to the modified cellulose scaffold material. Groups of cells were well stretched, lining pores of the mineralized scaffolds (Fig. 6d). A greater amount of F-actin is highlighted lining the pores, as there is extensive cell clustering and copious amount of cytoskeleton. On the mineralized surface without the pores, there is cell stretching, but there are distinct areas amongst the cells showing minimal overlap of F-actin. These results suggest that cells within the pores can better cluster, and this clustering results in additional cytoskeleton growth and stretching.

The cell density value of the unmodified scaffolds after 72 h of incubation was 16.6% lower than the initial seeded cell density (Fig. 7). This data provides evidence that cells were only partially able to attach to the unmodified cellulose surface. In contrast, for the modified scaffolds (PEC, MEC, and PMEC) cell density was slightly higher than the seeded cell density, which suggested that the cells attached to the surface and started to proliferate. These cell density values, quantified from the fluorescence micrographs, indicated that both scaffold modifications, porosity and mineralization, had a positive effect on MC3T3-E1 cell density. However, no synergistic effect for porosity and surface chemistry was observed for cell adhesion and proliferation after 3 days observation (Fig. 7). Because of the variability of the data, only the hydroxyapatite-modified scaffold is statistically different from the control ($p < 0.10$). Mechanisms for enhanced cell adhesion arising from hydroxyapatite treatment have been discussed in literature, but the studies suggest a number of different factors. Highlighted in these mechanisms is the process of partial solubilization of ions, followed by protein adsorption that facilitates cell binding (Bertazzo et al., 2010). Crystal orientation and enhanced surface area also have been implicated by enhancing adsorption of cell adhesion peptides (Hagio et al., 2009; Okamoto, Matsuura, Hosokawa, & Akagawa, 1998). Overall, these studies highlight the importance of hydroxyapatite surface chemistry in enhancing cell adhesion.

4. Conclusions

In this study electrospun nanofibrous cellulose scaffolds with controlled micro-architecture and surface chemistry were fabricated by post-treatment processing with a CO_2 laser and phosphate buffered saline solution. Laser ablation impacted the irradiated area, leaving the bulk of the material unmodified by the treatment. This treatment offers a unique route to design porosity into scaffolds leaving the electrospun fibers intact a few micrometers away from the pore edge. Furthermore, surface chemistry was controlled via mineralization in phosphate buffered saline. Ca–P mineralization took place on the fiber surface resulting in a similar diffraction pattern to HA as a result of this alternative solution compared to simulated body fluid. The biomimetic mineralization and macro porosity induced a positive effect on cell adhesion and spreading; however, a synergetic effect between these two treatments was not observed. The design and fabrication method offers integration of microscale porosity with fibrous biopolymers that mimics native extracellular architecture. This technology may also be combined with other scaffold methods like three-dimensional weaving, in order to enhance porosity to enable seeding and vascularization to enhance tissue scaffold design.

Acknowledgements

This work was supported by the Knut and Alice Wallenberg Foundation through the Wallenberg Wood Science Center of Sweden, the United States Department of Agriculture NIFA NRI (grant 2010-65504-20429), and the Institute of Critical Technology and Applied Science, Blacksburg, VA. The authors wish to thank Mr. W. Travis Church for assistance with laser operation.

Appendix A. Supplementary data

Supplementary data associated with this article can be found, in the online version, at http://dx.doi.org/10.1016/j.carbpol.2012.12.037.

References

Bertazzo, S., Zambuzzi, W. F., Campos, D. D., Ogeda, T. L., Ferreira, C. V., & Bertran, C. A. (2010). Hydroxyapatite surface solubility and effect on cell adhesion. *Colloids and Surfaces B: Biointerfaces*, *78*(2), 177–184.

Bodin, A., Bharadwaj, S., Wu, S., Gatenholm, P., Atala, A., & Zhang, Y. (2010). Tissue-engineered conduit using urine-derived stem cells seeded bacterial cellulose polymer in urinary reconstruction and diversion. *Biomaterials*, *31*(34), 8889–8901.

Buttafoco, L., Kolkman, N., Engbers-Buijtenhujis, P., Poot, A., Dijkstra, P., Vermes, I., et al. (2006). Electrospinning of collagen and elastin for tissue engineering applications. *Biomaterials*, *27*(5), 724–734.

Carrillo, F., Colom, X., Suñol, J., & Saurina, J. (2004). Structural FTIR analysis and thermal characterisation of lyocell and viscose-type fibres. *European Polymer Journal*, *40*(9), 2229–2234.

Chen, V., Smith, L., & Ma, P. (2006). Bone regeneration on computer-designed nanofibrous scaffolds. *Biomaterials*, *27*(21), 3973–3979.

Czaja, W., Krystynowicz, A., Bielecki, S., & Brown, R. (2006). Microbial cellulose – The natural power to heal wounds. *Biomaterials*, *27*(2), 145–151.

Czaja, W., Young, D., Kawecki, M., & Brown, R. (2006). The future prospects of microbial cellulose in biomedical applications. *Biomacromolecules*, *8*(1), 1–12.

Gilbert, M., Shaw, W., Long, J., Nelson, K., Drobny, G., Giachelli, C., et al. (2000). Chimeric peptides of statherin and osteopontin that bind hydroxyapatite and mediate cell adhesion. *Journal of Biological Chemistry*, *275*(21), 16213–16218.

Grafahrend, D., Heffels, K., Beer, M., Gasteier, P., MAller, M., Boehm, G., et al. (2011). Degradable polyester scaffolds with controlled surface chemistry combining minimal protein adsorption with specific bioactivation. *Nature Materials*, *10*(1), 67–73.

Hagio, T., Tanase, T., Akiyama, J., Umino, M., Iwai, K., & Asai, S. (2009). Difference in bioactivity, initial cell attachment and cell morphology observed on the surface of hydroxyapatite ceramics with controlled orientation. *Materials Transactions*, *50*(4), 734–739.

Hofmann, I., Müller, L., Greil, P., & Müller, F. (2006). Calcium phosphate nucleation on cellulose fabrics. *Surface and Coatings Technology*, *201*(6), 2392–2398.

Hollister, S. J. (2005). Porous scaffold design for tissue engineering. *Nature Materials*, *4*(7), 518–524.

Karageorgiou, V., & Kaplan, D. (2005). Porosity of 3D biomaterial scaffolds and osteogenesis. *Biomaterials*, *26*(27), 5474–5491.

Karande, T., Ong, J., & Agrawal, C. (2004). Diffusion in musculoskeletal tissue engineering scaffolds: Design issues related to porosity, permeability, architecture, and nutrient mixing. *Annals of Biomedical Engineering*, *32*(12), 1728–1743.

Li, W., Laurencin, C., Ctaerson, E., Tuan, R., & Ko, F. (2002). Electrospun nanofibrous structure: A novel scaffold for tissue engineering. *Journal of Biomedical Materials Research*, *60*(4), 613–621.

Lim, Y., Johnson, J., Fei, Z., Wu, Y., Farson, D., Lannutti, J., et al. (2011). Micropatterning and characterization of electrospun poly(ε-caprolactone)/gelatin nanofiber tissue scaffolds by femtosecond laser ablation for tissue engineering applications. *Biotechnology and Bioengineering*, *108*(1), 116–126.

Liu, H., & Hsieh, Y. (2002). Ultrafine fibrous cellulose membranes from electrospinning of cellulose acetate. *Journal of Polymer Science Part B: Polymer Physics*, *40*(18), 2119–2129.

Ma, Z., & Ramakrishna, S. (2008). Electrospun regenerated cellulose nanofiber affinity membrane functionalized with protein A/G for IgG purification. *Journal of Membrane Science*, *319*(1–2), 23–28.

Ma, Z., Kotaki, M., & Ramarkrishna, S. (2005). Electrospun cellulose nanofiber as affinity membrane. *Journal of Membrane Science*, *265*(1–2), 115–123.

Malda, J., Woodfield, T., van del Vloodt, F., Kooy, F., Martens, D., Tramper, J., et al. (2004). The effect of PEGT/PBT scaffold architecture on oxygen gradients in tissue engineered cartilaginous constructs. *Biomaterials*, *25*(26), 5773–5780.

McCullen, S., Miller, P., Phillip, R., Gittard, S., Gorga, R., Pourdeyhimi, B., et al. (2010). In situ collagen polymerization of layered cell-seeded electrospun scaffolds for bone tissue engineering applications. *Tissue Engineering Part C: Methods*, *16*(5), 1095–1105.

Murdock, C. C. (1930). The form of the X-ray diffraction bands for regular crystals of colloidal size. *Physical Review*, *35*(1), 8–23.

Ogino, M., Ohuchi, F., & Hench, L. (1980). Compositional dependence of the formation of calcium phosphate films on bioglass. *Journal of Biomedical Materials Research*, *14*(1), 55–64.

Ohtsuki, C., Kushitani, H., Kokubo, T., Kotani, S., & Yamamuro, T. (1991). Apatite formation on the surface of ceravital-type glass-ceramic in the body. *Journal of Biomedical Materials Research*, *25*(11), 1363–1370.

Okamoto, K., Matsuura, T., Hosokawa, R., & Akagawa, Y. (1998). RGD peptides regulate the specific adhesion scheme of osteoblasts to hydroxyapatite but not to titanium. *Journal of Dental Research*, *77*(3), 481–487.

Posner, A., & Betts, F. (1975). Synthetic amorphous calcium phosphate and its relation to bone mineral structure. *Accounts of Chemical Research*, *8*(8), 273–281.

Rebollar, E., Cordero, D., Martins, A., Chussi, S., Reis, R., Neves, N., et al. (2011). Improvement of electrospun polymer fiber meshes pore size by femtosecond laser irradiation. *Applied Surface Science*, *257*(9), 4091–4095.

Rodriguez, K., Renneckar, S., & Gatenholm, P. (2011). Biomimetic calcium phosphate crystal mineralization on electrospun cellulose-based scaffolds. *ACS Applied Materials and Interfaces*, *3*(3), 681–689.

Stevens, M., & George, J. (2005). Exploring and engineering the cell surface interface. *Science*, *310*(5751), 1135–1138.

Svensson, A., Nicklasson, E., Harrah, T., Panilaitis, B., Kaplan, D., Brittberg, M., et al. (2005). Bacterial cellulose as a potential scaffold for tissue engineering of cartilage. *Biomaterials*, *26*(4), 419–431.

Tas, A. C. (2000). Synthesis of biomimetic Ca-hydroxyapatite powders at 37 °C in synthetic body fluids. *Biomaterials*, *21*(14), 1429–1438.

Zimmermann, K., LeBlanc, J., Sheets, K., Fox, R., & Gatenholm, P. (2011). Biomimetic design of a bacterial cellulose/hydroxyapatite nanocomposite for bone healing applications. *Materials Science and Engineering: C*, *31*(1), 43–49.

Zong, X., Bien, H., Chung, C., Yin, L., Fang, D., Hsiao, B., et al. (2005). Electrospun fine-textured scaffolds for heart tissue constructs. *Biomaterials*, *26*(26), 5330–5338.